THE GAS DYNAMICS OF THE EXHAUST DIFFUSERS: COMPUTATIONAL ASPECTS

VALERY G. SOLODOV

Theoretical Mechanics and Hydraulics Department,
Kharkov State Technical University,
Petrovsky 25, 61002 Kharkov, Ukraine
solodov@khadi.kharkov.ua

Abstract: Some recent advances in computational gas dynamics of exhaust diffusers are presented. The compressor/turbine axial-radial exhaust diffusers and outlet devices of compressor/turbine units, exhaust hoods for power steam turbines are considered. The peculiarities of gas dynamics of the above mentioned devices are discussed. The formulations of problems for CFD analysis of these devices are discussed including the coupling procedure for joint operation of the last stage and exhaust hood. The numerical method and the implementation of a differential turbulence model are described. The new approach to the description of computational domain and parallel numerical solution of transport equations based on the unstructured set of structured grid blocks is also presented.

1. Introduction

The analysis of possible ways of design improvements in axial turbomachines shows that the reserves of stage efficiency increase from reblading are moderate. The outlet and exhaust diffusers have essential reserves of efficiency rise because of significant pressure losses provoked by flow separation of high intensity. The operational reliability of turbomachines depends on aerodynamic characteristics of outlet devices. Circular nonuniformity of parameters influences the vibration characteristics of the last stage blading, condenser or combustion operation. The diffusers are difficult to improve aerodynamically, and the questions concerning flow simulation in them are the subject of our consideration.

2. Mathematical flow modelling through channels of complex shape

2.1. Basic equations governing fluid flow

The calculation of viscous compressible diffuser flow through the 3D channels of complex shape requires the numerical integration of the full form of compressible time dependent Navier-Stokes equations averaged after Reynolds-Favre [1]. Following the

technique of Reynolds-Favre averaging for Navier-Stokes equations (RANS) in integral form relative mean values of gas-dynamic variables can be written as:

$$\int_V \frac{\partial \rho}{\partial t} dV + \oint_S \rho \vec{u} \cdot \vec{n} dS = 0$$

$$\int_V \frac{\partial (\rho \vec{u})}{\partial t} dV + \oint_S \rho \vec{u}(\vec{u} \cdot \vec{n}) dS + \oint_S \widehat{\tau} \cdot \vec{n} dS = 0$$

$$\int_V \frac{\partial (\rho E)}{\partial t} dV + \oint_S \rho E(\vec{u} \cdot \vec{n}) dS + \oint_S \vec{u}(\widehat{\tau} \cdot \vec{n}) dS - \oint_S (\vec{q} \cdot \vec{n}) dS = 0. \qquad (1)$$

State equation of perfect gas reads as:

$$p = R\rho T.$$

Total shear stresses are divided into laminar and turbulent part:

$$\tau_{ij} = \tau_{ij\,lam} + \tau_{ij\,tur},$$

$$\tau_{ij\,lam} = 2\mu_{lam}(S_{ij} - S_{\alpha\alpha}\delta_{ij}/3)$$

, where $S_{ij} = 0.5\left(\frac{\partial u_i}{\partial x_j} + \frac{\partial u_j}{\partial x_i}\right)$.

The Reynolds turbulence stresses obtained after the averaging procedure are subject to turbulence modelling techniques.

If the Boussinesq hypothesis used for modelling the turbulence stresses could be represented in terms of the eddy viscosity in analogy with Stoke's law for the molecular stresses, then:

$$\tau_{ij\,tur} = -\overline{\rho u'_i u'_j} = 2\mu_{tur}(S_{ij} - S_{\alpha\alpha}\delta_{ij}/3) - 2\rho k\delta_{ij}/3,$$

where $k = 0.5\,\overline{u'_i u'_j}$ is the kinetic turbulence energy.

Heat flux rates read as:

$$q_j = q_{j\,lam} + q_{j\,tur} = -(\kappa_{lam} + \kappa_{tur})\frac{\partial T}{\partial x_j}.$$

The turbulent heat transfer rates are modeled in correspondence with Fourier's laminar flow law in terms of the eddy thermal conductivity.

2.2. Navier-Stokes numerical algorithm

The majority of results described in this study were obtained using the code [2], which solves a time dependent form of three-dimensional RANS equations written in a generalized coordinate system, using a time marching numerical formulation.

The RANS equations are solved numerically using the Godunov-type upwind differencing [3], which does not need additional artificial diffusion to obtain the convergence of the algorithm. The cell-centered finite volume difference scheme applies ENO (essentially non-oscillating) reconstruction [4] for convective derivatives, which ensures second order spatial accuracy everywhere and third-order accuracy locally. The approximation of viscous derivatives is provided with the use of second order central differences. The computational efficiency is increased due to the implementation of a delta-form implicit operator of Beam-Warming [5] used as a corrector stage. A more detailed description of the difference scheme can be found in [3, 4, 6].

2.3. Turbulence modelling

Being in frame of the Boussinesq hypothesis, the well-known differential turbulence models [7] are convenient for implementation, because they can be expressed in the form of the transport equation. The implementation of the one-equation Spalart-Allmaras (S-A) turbulence model [8] is discussed bellow.

The S-A differential turbulence model is the low Reynolds model represented by one differential equation. It shows excelent results in comparison with other models [7], and is more efficient in implementation.

According to [8] the governing equation for the kinematic eddy viscosity variable $\tilde{\nu}$ can be written as:

$$\frac{D(\rho\tilde{\nu})}{Dt} = \frac{\partial\rho\tilde{\nu}}{\partial t} + \nabla\cdot(\rho\tilde{\nu}\vec{u}) = P + V - D + T, \tag{2}$$

where $P = C_{b1}(1 - f_{t2})\rho\tilde{S}\tilde{\nu}$, $D = \left[C_{w1}f_w - \frac{C_{b1}}{k^2}f_{t2}\right]\cdot\rho\left(\frac{\tilde{\nu}}{d}\right)^2$ are the turbulence production and destruction terms, respectively; $V = \frac{1}{\sigma}\left[\nabla\cdot(\rho(\nu_{lam} + \tilde{\nu})\nabla\tilde{\nu}) + C_{b2}\rho(\nabla\tilde{\nu})^2\right]$ is the diffusive term; $T = f_{t1}\rho\Delta U^2$ is the flow turbulence transition term.

The eddy viscosity μ_{tur} is given by the transformation: $\mu_{tur} = \rho\tilde{\nu}f_{v1}$, where $f_{v1} = \chi^3/(\chi^3 + C_{v1}^3)$ is a smoothing function for the kinematic viscosity ratio $\chi \equiv \tilde{\nu}/\nu_{lam}$.

The auxiliary relations written below to complete the model include: $\tilde{S} = \Omega + \tilde{\nu}f_{v2}/(kd)^2$, where d is the distance to the nearest wall, $f_{v2} = 1 - \chi/(1 + \chi f_{v1})$, $\Omega = |\nabla\times\vec{v}|$ is the magnitude of vorticity; and $f_w = g\left[(1 + C_{w3}^6)/(g^6 + C_{w3}^6)\right]^{1/6}$, $g = r + C_{w2}(r^6 - r)$, $r \equiv \tilde{\nu}/(\tilde{S}(kd)^2)$.

The transition term describes the transition process from the laminar regime to the turbulent one, if the external flow initially is not turbulent. The model generates the turbulent viscosity in the flow region under a very small input value given in the initial inlet boundary condition $(0.1\nu_{lam})$, so the transition term usually is omitted [7]. The original constants for this model are given in [8].

2.4. Turbulence model implementation

The original S-A transport equation describes the convective transfer of pseudoviscosity. It is basically of similar form as Equation (1) and so can be solved by the same difference scheme and the technique mentioned. The Rieman problem for this transport equation can be resolved to determine the turbulent viscosity flux through the cell walls.

In order to match the finite volume approach proposed, it is better to rearrange the original S-A transport equation, in view of its application to the implicit part of the scheme:

$$\frac{D(\rho\tilde{\nu})}{Dt} = C_{b1}(1 - f_{t2})\rho\tilde{S}\tilde{\nu} + \frac{\rho}{\sigma}\left[\nabla\cdot((\nu + (1 + C_{b2})\tilde{\nu})\nabla\tilde{\nu}) - C_{b2}\tilde{\nu}\nabla^2\tilde{\nu}\right] -$$
$$\left[C_{w1}f_w - \frac{C_{b1}}{k^2}f_{t2}\right]\cdot\rho\left(\frac{\tilde{\nu}}{d}\right)^2 + f_{t1}\rho\Delta U^2 .$$

After application of generalized coordinate transformation the explicit part of this equation is realised as the governing equations, *i.e.* the transport equation is decomposed into the convective and diffusive fluxes through the hexahedral cell surfaces; the sources such as destruction and transition terms are represented as cell centered averaged values. Explicit approximation of the S-A transport equation reveals a small interval of stability, so the implicit-in-time performance for the convective and diffusive terms is recommended [7, 8].

Some solvers [7, 9] apply the first order approximation of $\rho\tilde{v}$ cell reconstruction to ensure the stability of the scheme for this equation.

The main difference in comparison with Equation (1) consists in the presence of a group of source terms with different nature and mathematical structure. Namely, the diffusive first order term V can be implemented in the left hand side of equation and calculated by splitting along three independent directions with the use of partial gas-dynamic derivatives. The production, destruction and transition terms are calculated locally as cell averages and implemented implicitly. For the implicit part, a simple linearization of source terms is performed.

The numerical performance of source terms of this equation is of major importance for the stability of the scheme. In correspondence with the original paper [8] the sum of source terms is linearized. The method used here corresponds in general to the 4th method of that reference. Because of strongly nonlinear behavior of these terms it is desirable to linearize them when their sum increases the diagonal dominance of the implicit matrix coefficient. So, the following representation of simple linearization in time for the source terms could be effective:

$$\delta^{n+1}[P-D] = -\left(\frac{P-D}{\rho\tilde{v}}\right)^n (\rho\tilde{v}^{n+1} - \rho\tilde{v}^n).$$

In the examples of this paper, flow is supposed to be fully turbulent, which could be ensured by inlet boundary conditions, so a trip function represented in the model equation by term T is not used in the model.

2.5. *Stability analysis and convergence acceleration technique*

Explicit part of the numerical scheme is limited following the CFL-condition for the convective operator of Godunov's type [9]. The application of the implicit Beam-Warming operator admits for majority of flows to increase the Courant number by 10–12 times.

The time step is a function of the cell minimum dimension, so for steady state calculations the local time stepping is used.

The differential turbulence models based on one or two equations make some restriction on the value of the stability criterion. It depends on the type of turbulence model and general stability of difference scheme. S-A model with TVD schemes requires additional subiterations in time within the time step of the basic scheme. Godunov's type scheme [4] in the case of low values of initial turbulence and for the starting period of calculations requires usually one or two subiterations. An alternative solution is the individual time lag technique for the turbulence pseudo-viscosity equation [10], which permits us to avoid subiteration and ensures the accuracy of steady state modelling.

2.6. *Unstructured multiblock topology of computational region*

The uniform numerical technique for multiblock CFD-solver proposed in [11] (see also [12]) to integrate the RANS and turbulence model equations on the structured description of the computational region is modified in this paper.

In correspondence with the original version [11], the 3D algorithm is split, both for the explicit and implicit parts, into three independent directions in correspondence with three families of faces of hexahedral cells, and calculations are executed uniformly for all the cells and sequentially for all the directions. The algorithm has certain analogy with the process of textile weaving with *threads* in the region with complex configuration of boundaries.
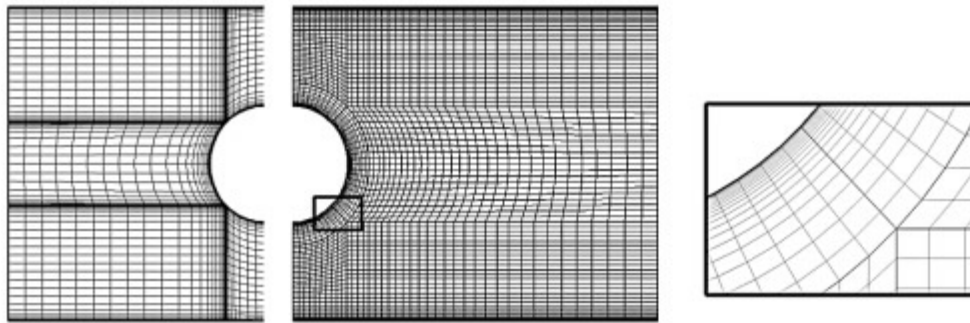
Figure 1. Tightly fitting meshing samples

According to [12] the preprocessor generates the association of threads of every family, named by *chain*, taking into account the structure of every domain of the whole region. The chain of each of the three families is processed by solver sequentially along the three independent directions in such a way that every cell is run three times and the difference approximation of every equation in each cell for a time-step is fulfilled.

This approach can directly be applied to structured meshes of H-, C-, O-types. In the case of a region of complex shape, a combination of the above mentioned meshes may occur, which leads to a deviation of meshes exponentially condensed at the walls. Certain difficulty of the approach consists in the necessity to apply the interpolation procedure on the internal boundaries of meshes between the domains or groups of domains of different texture or meshing topology.

In the present paper the development of this approach is proposed, which introduces tightly fitting meshes independently of the domain structure (Figure 1). This modification permits us to apply the exponentially condensing meshes tightly fitting all rigid boundaries by analogy to physical boundary layers and allows us to use 3D structured meshes of H-, C-, O-types in the domains.

The advantages of the modification proposed are:

- relatively uniform meshing in the flow kernel independent of the complexity of the region;
- ensuring the acceptable meshing parameters in the boundary layer;
- no necessity of interpolation between the chains.

This technique also provides the economy of computational resources and the adequate description of flow physics both in the kernel and in the boundary layer due to the possibility of using 3D structured meshes of H-, C-, O-types in different domains of the computational region.

The decomposition of the computational region into threads is accomplished in the code [10] on the preprocessor level, the reconstruction of the region and computational results are executed by the postprocessor.

An important feature of the technique proposed is its versatility and generality of mesh systems upon which the analysis may be performed. The code permits the use of a multiple-block mesh discretization, which provides high flexibility for analysing complex geometry. The thread-tightly fitting meshing technique enables the joining of complex, multiple-region domains without overlapping grid interface boundaries.

2.7. Parallelization

The organization of the solver proposed permits us to use effectively the decomposition of the computations on the parallel processes for the computational platform with several CPU. On the contrary, the structure of the code is not determined by the requirements of parallelization, namely, the block topology and thread organization determine the code structure.

To perform the parallelization, an individual subprocess can be created which operates simultaneously with one thread only or the proportional count of threads. These two strategies are able to use effectively the arbitrary number of processors and can be performed at any platform.

2.8. Conditions at the boundaries of computational region

For the inlet part of the boundaries, the total energy, direction of velocity vector and entropy function distributions are formulated. For the outlet part, the static pressure distribution is formulated. For the turbulence model equation, the inlet boundaries require the pseudoviscosity value as an initial value of turbulence, which could make a part of the laminar viscosity. At the vicinity of the outlet boundaries, the pseudoviscosity is a constant. At the rigid boundaries the usual non-slip condition is used [6].

2.9. Numerical tests

In order to demonstrate the efficiency of the numerical algorithm and turbulence model, examples of viscous flow simulation are presented below. The figures illustrate the running results of test cases that were performed to ensure the model accuracy. The typical CPU time for one Intel Pentium III 650 MHz processor is $(3.3–3.9) \cdot 10^{-5}$ sec/cell/cycle. For a dual CPU system the time is diminished by 1.8–1.9.

The first test case presented (Figures 2–5) is the subsonic flow through the strongly curvilinear U-duct with experimental data [13]. The nominal Mach number is $Ma = 0.1$, the Reynolds number is $Re = 26.0 \cdot 10^6$. The cross-flow finest grid is 150 points that yields the minimum spacing at the wall about $1.0 \cdot 10^{-5}$ cm and the y^+ value of less than 0.2. The location and extent of separation are: 168° versus 150° (data [13]); separation length $l/H = 1.57$ *vs.* 1.26–1.76 [3]; reattachment $x/H = 1.47$ *vs.* 1.0–1.5 ([13]).

The second test case presented (Figure 6) is the transonic flow over the axially symmetric bump compared with experimental data [14]. A subsonic flow with $Ma = 0.875$ and $Re = 13.1 \cdot 10^6$ accelerates over a bump creating a shock wave with a recirculation zone behind the shock. The cross-flow finest grid is 100 points that yields the minimum spacing at the wall about $7.0 \cdot 10^{-5}$ cm. The format of the presented results is replicated from the cited references to better complement the existing knowledge base.

3. Flow simulation through axial-radial diffusers and exhaust hoods

The aerodynamic improvement of the turbine and compressor exhaust diffusers by means of CFD is a problem successfully solved during the last decade [15–18, 9]. There are some specific problems, which distinguish the flow simulation through axial-radial diffusers and arbitrary curvilinear channels. The low-pressure recovery, considerable pressure losses, developed flow separation bubbles with reverse flow from the outflow boundary to the inlet, or aerodynamic flow instability are among them.
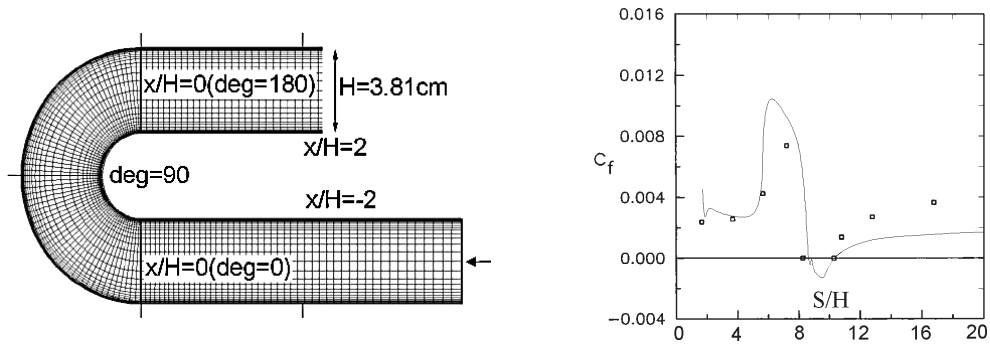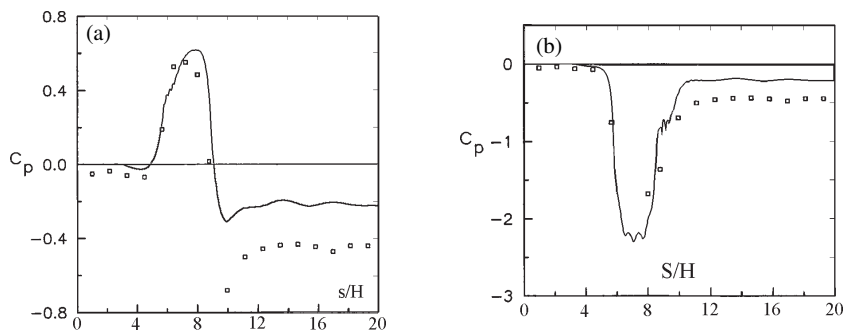
Figure 2. Inner surface skin friction coefficient

Figure 3. (a) Outer surface pressure coefficient; (b) Inner surface pressure coefficient
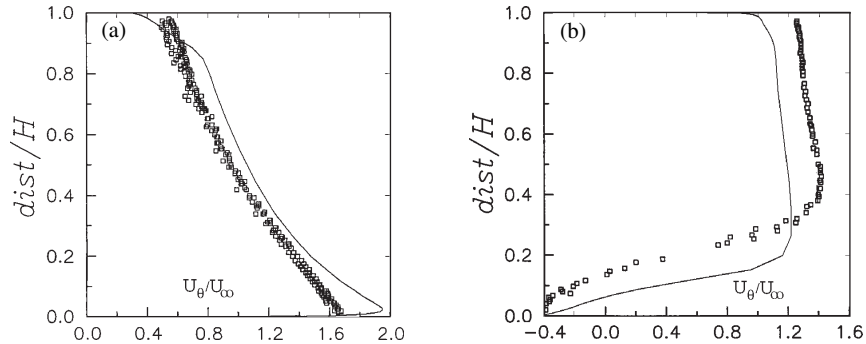

Figure 4. (a) Streamwise velocity at 90° in the bend;
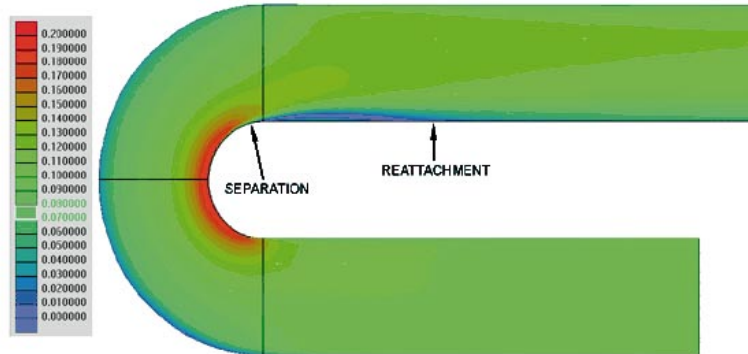(b) Streamwise velocity at $x/H = 0.5$ in the separated region

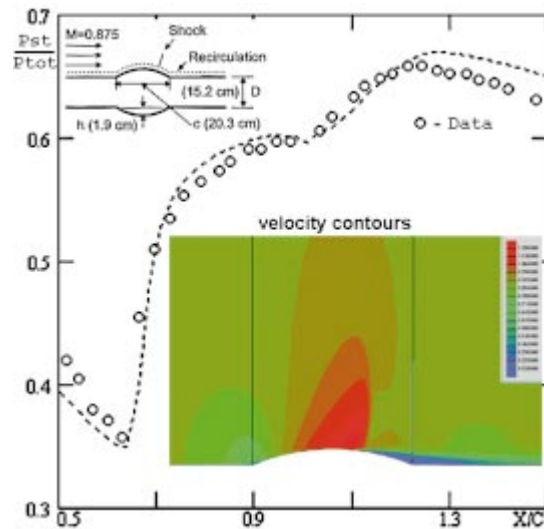**Figure 5.** Velocity contours in curvilinear U-duct

Figure 6. Static pressure and Mach numbers near axisymetric bump

3.1. *Isolated compressor and turbine exhaust diffusers*

According to experimental data [19] the axial-radial compressor diffusers of the same external dimensions have a difference in full pressure losses by 1.5–2.0 times depending on the profiling law, so the possibilities for their aerodynamic improvement exist.

Full pressure losses for the axial-radial diffusers consist of internal losses and outlet velocity losses. When the diffuser operates jointly with the casing its outlet velocity losses cannot be added to the loss balance of the whole exhaust system. Diminishing the outlet velocity losses indirectly effects the aerodynamic characteristics of the exhaust device due to diminishing of exhaust nonuniformity. When the pressure recovery occurs due to diminishing of internal losses, the diminishing of full losses for the isolated diffuser and exhaust device is approximately the same. In this case the study of the isolated diffuser for aerodynamic improvement is especially desired.

Taking into account recent advances in CFD, flow simulation in compressor and turbine axial-radial diffusers requires full N-S analysis, accurate turbulence stresses modelling and adequate realisation of inlet and outlet boundary conditions.

In some cases the inverse swirl flow can appear at the outlet or at another boundary as a separation region, as it usually occurs for radial diffusers, exhaust pipes, exhaust hoods and other aerodynamically imperfect devices. So, certain part of the outlet boundary is physically the inlet one and requires the formulation of the inlet condition, *i.e.* certain values of the total pressure and temperature.

The examples of flow simulation for compressor diffusers are presented below. Reattached and detached flow separation are considered at the outer diffuser contour. The test cases presented (Figures 7 and 8) are subsonic flows through a series of compressor diffusers with experimental data [19] regarding the full losses. The nominal Mach numbers are Ma = 0.4–0.6, the Reynolds numbers are within Re = $1.1 \cdot 10^5$–$1.4 \cdot 10^6$. The cross-flow finest grid is 80 points that yields the minimum spacing at the wall about $1.5 \cdot 10^{-6}$ m and the y^+ value of less than 2.5. The calculation region contains (consists of) a 4 cell sector in the circular direction and the calculations were done under the angular periodicity condition.
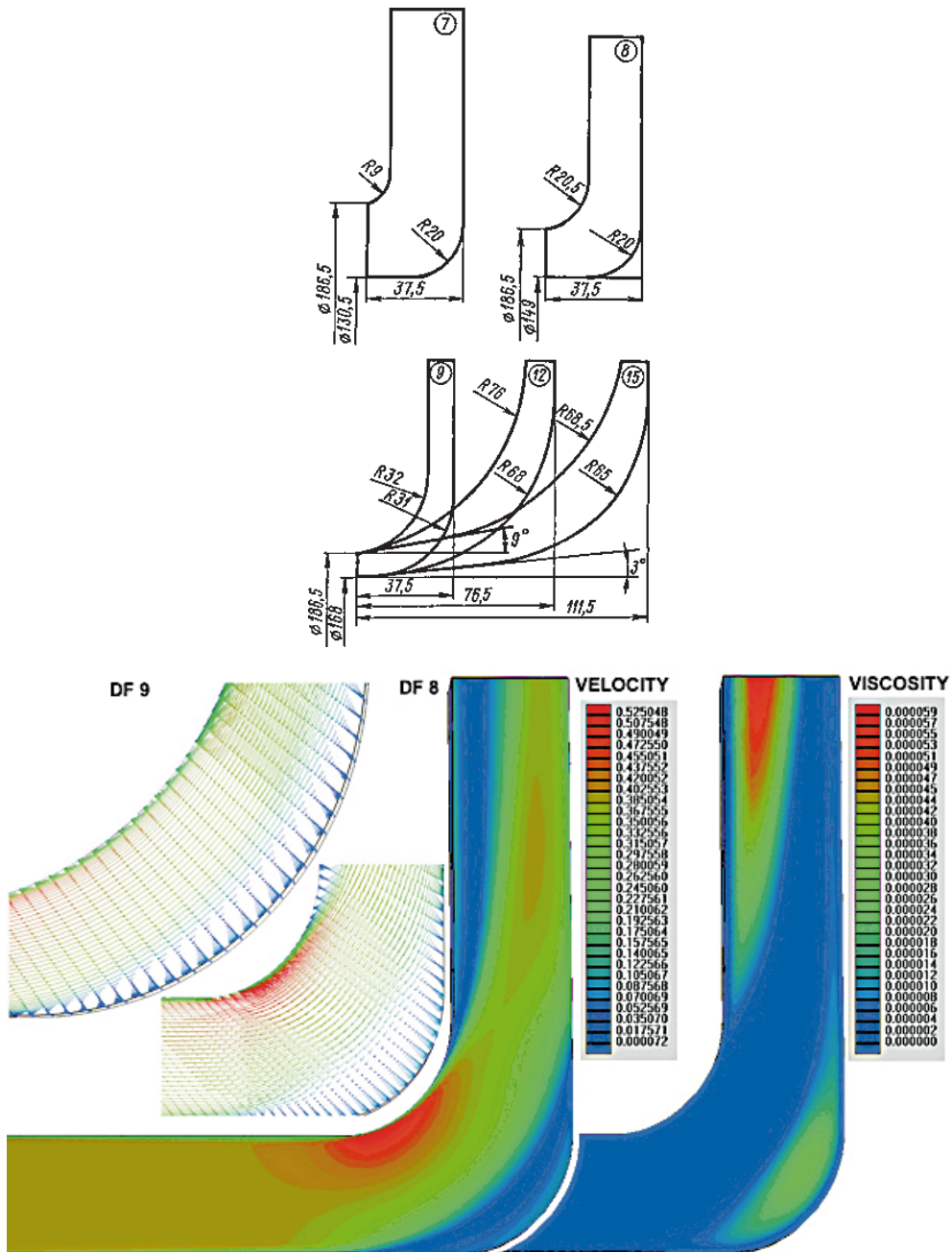
Figure 7. Flow in diffusers No. 8,9 for $Ma_{inlet} = 0.4$–0.47, $Re = (1.1$–$1.6) \cdot 10^6$

The inlet flow was considered of low turbulence level with $\tilde{\nu} = 0.1\nu_l$. Calculated full losses for diffusers with reattached flow separation better correspond to experimental data [19] than for the cases with open flow separation into the outlet boundary. One reason consists in incomplete information regarding the experimental conditions. The second one could be because of inadequate boundary data formulation: namely, distributions of flow angle, total pressure and temperature for the suction part of the outlet boundary.
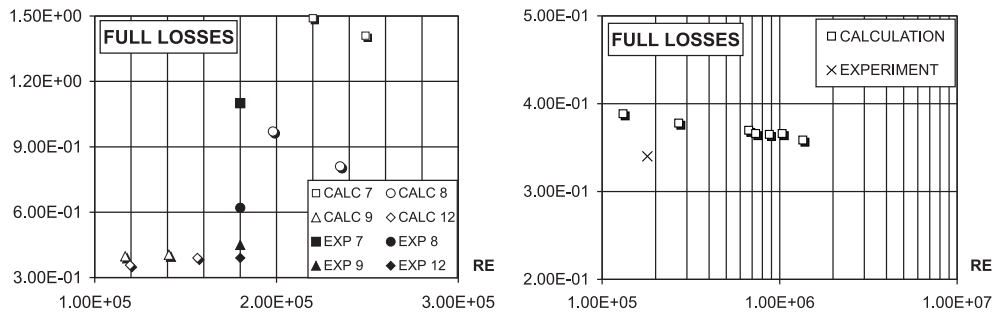
Figure 8. Full losses in diffusers No. 7–15

Exhaust diffusers of turbines for power generation provide for bleeding of steam to the condenser. The coefficient of full losses for the exhaust system exceeds as a rule 1.0 [19–21]. This one can be explained by peculiarities of velocity flow field behind the last stage and because of flow pattern under the casing. The typical velocity distribution in the diffuser inlet [21–23] is determined by the design philosophy and functional specification of the last stage. Even for partial regimes up to 60% of the operational regime, the velocity in inlet peripheral layers of the diffuser increases to supersonic values because of the tip clearance jet [20]. The supersonic region interacts with the stream kernel, leads to the developed flow separation which diminishes the effective outlet area of the diffuser.

For certain regimes and diffuser geometry, the periodic shock wave occurs [22, 23] along the outer diffuser shell which provokes the dynamic deformation, periodic change of inlet/outlet flow rate and inverse dynamic effect on the last stage blading. Total pressure losses of the last compartment essentially rise. The presence and geometrical characteristics of the casing influence the decrement of oscillatory phenomena in the diffuser [18, 22–26].

The one-side steam exhaust into the condenser causes flow turning and its part curls up into two vortex jets. These vortex jets induce a large intensity secondary flow, stimulating the rise of losses in the exhaust chamber. For highly loaded turbine operational regimes and high inlet velocities in the diffuser, the choking occurs whose occurrence is determined by the level of losses in the exhaust hood [21].

The above mentioned factors emphasize that aerodynamic study of diffusers is more valuable when coupled with the exhaust chamber than for the isolated model.

Numerical investigations of exhaust hoods are represented by works of the last decade [1, 15, 17, 25–38]. The keynote work of EPRI [33] should be marked which proposed in 1995 the Program of Low Pressure Steam Turbine Thermal Performance Improvements with wide application of CFD. In works [21, 29] the experience was summarized on modernization of hoods of old design with the use of CFD analysis. Certain advances were achieved in study of oscillatory phenomena in exhaust hoods [22, 24, 26]. During the last five years the modern differential turbulence models [6–8] have been tested, power workstations have been created making possible the implementation of CFD analysis into exhaust hood specification.

The author's experience in flow simulation of turbomachinery exhaust systems is briefly presented below in examples of a gas turbine exhaust pipe [39], compressor outlet

chamber for gas pump units [40], the turbine exhaust hoods of the modern model and old-design 200 MW turbine [32]. The samples of tightly fitting meshes for flow paths of the above devices are shown in Figures 9 and 10.

The model of modern exhaust system of the Kharkov Turbine Plant (Figure 9) represents a free exhaust hood. The model is formed by 180 domains, the fine level mesh is near 579 000 cells. The exhaust system of a K-200-130 old-design 200 MW turbine produced in Poland licensed from Russia as a free hood is formed by 196 domains, the fine level mesh is near 587 000 cells. The outlet chamber (Figure 10) contains 157 domains and is described by a fine mesh of 590 000 cells. The exhaust pipe (Figure 10) is a curvilinear duct with a central rotational body behind the last gas turbine stage, and contains 13 symmetric blades. The geometry description needed the use of more than 555 domains, the fine level mesh is near 835 000 cells. For all meshes the ratio h_{max}/h_{min} is not less than $2.0 \cdot 10^3$. Some samples of flow visualization in these devices under model inlet/outlet conditions are shown in Figures 11 and 12. A series of calculations made for NPP Mashproekt [39] show the correspondence between the predicted and experimental data regarding the full pressure losses (main discrepancies are equal to 10–30%) and outlet parameter distributions.

The exhaust system of the old-design K-200-130 turbine was also studied experimentally in the framework of a program of modernization [32], and using the inviscid code [34]. This hood contained a large quantity of different scale internal elements such as walls with holes, blades, honeycomb *etc*. (Figures 13 and 14), so the viscous flow modelling met difficulties in description of the flow region, and was not performed for that stage.

The solver [34] allowed us to simulate the unsteady 3D flow in the hood with all main internal elements. The numerical analysis was used to determine the effectiveness of design decisions: putting into construction the asymmetrical diffuser with elliptic cut-off, whose side surfaces are mounted with negative covering with respect to the last stage blade; mounting a special honeycomb cascade in the pitch plane of the exhaust chamber; the system of modernized stiffening ribs with new holes to reduce the choking of the steam flow. The actual values of the parameters used in computations such as flow rate, inlet boundary distributions of flow parameters are taken from measurements carried out on a real turbine [32]; the rate of tip clearance flow amounting to about 10–15 per cent.

The flow modelling was done for subsequent selected new elements of the exhaust hood design and after the complete cycle of modernization. Such an approach permits us to evaluate the effect of every element, or step in design, on the change of spatial flow pattern. Analysing the predicted and experimental data one can see [29, 32] that the main features of the exhaust diffuser flow path and flow structure were qualitatively described:

- an aerodynamically non-perfect and short profile of the diffuser outer contour in the upper part;
- flow choking due to a relatively small area of the diffuser exhaust and space under the casing in this sector;
- the screening effect of the tip clearance jet in certain sectors;
- periodic choking of the lower part of the diffuser by a shock under regimes of inlet velocity level more than 0.5 Ma provoking oscillations of the flow rate.

The calculated frequencies were close to those obtained in the experiment [32]. The dangerous level of vibration was removed due to installation of the honeycomb to obtain a more rigid construction of the casing.
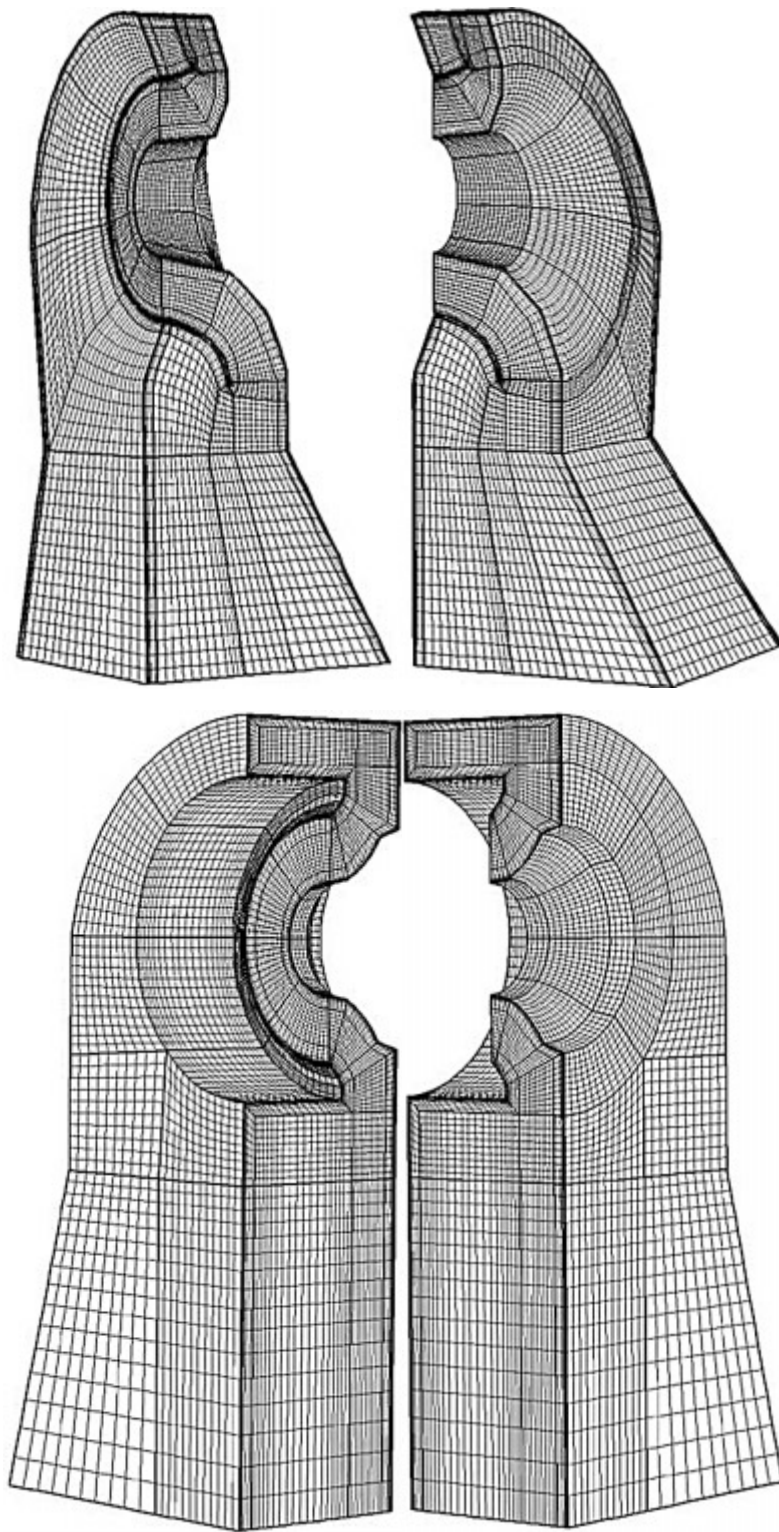
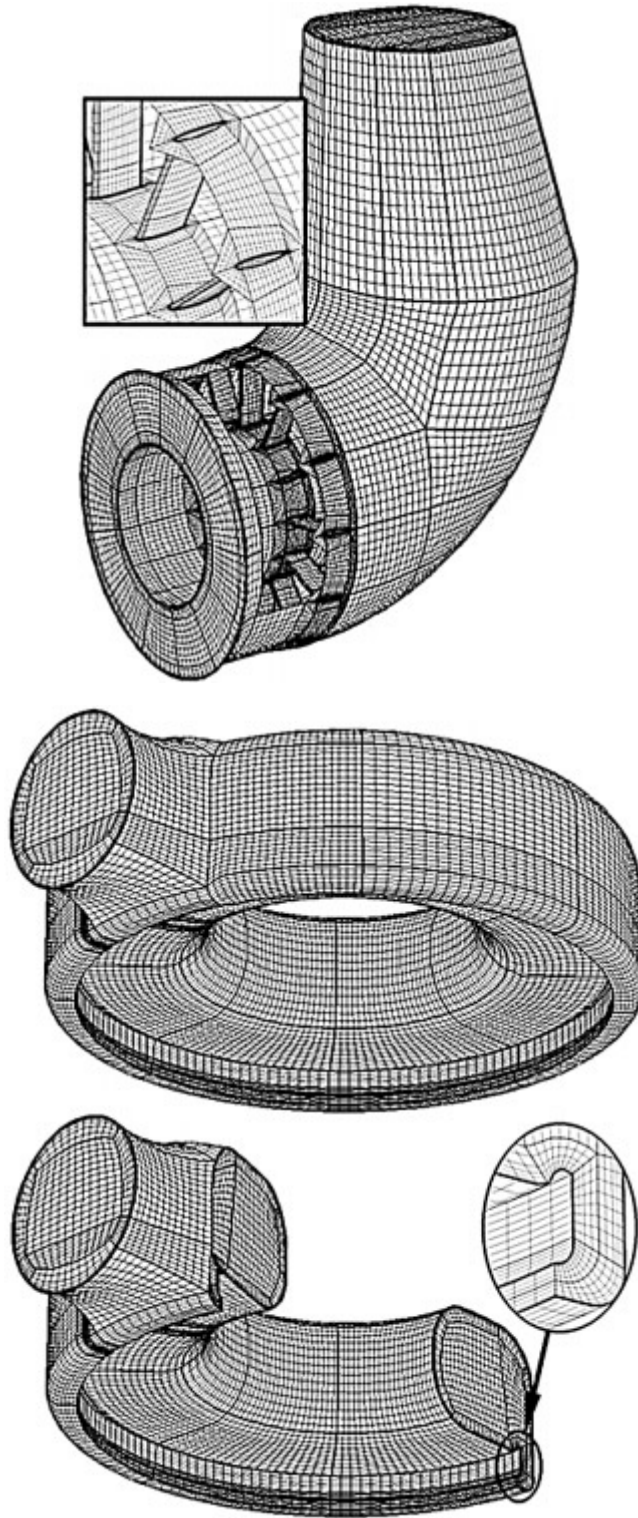**Figure 9.** Tightly fitting mesh for exhaust hoods of different design turbines

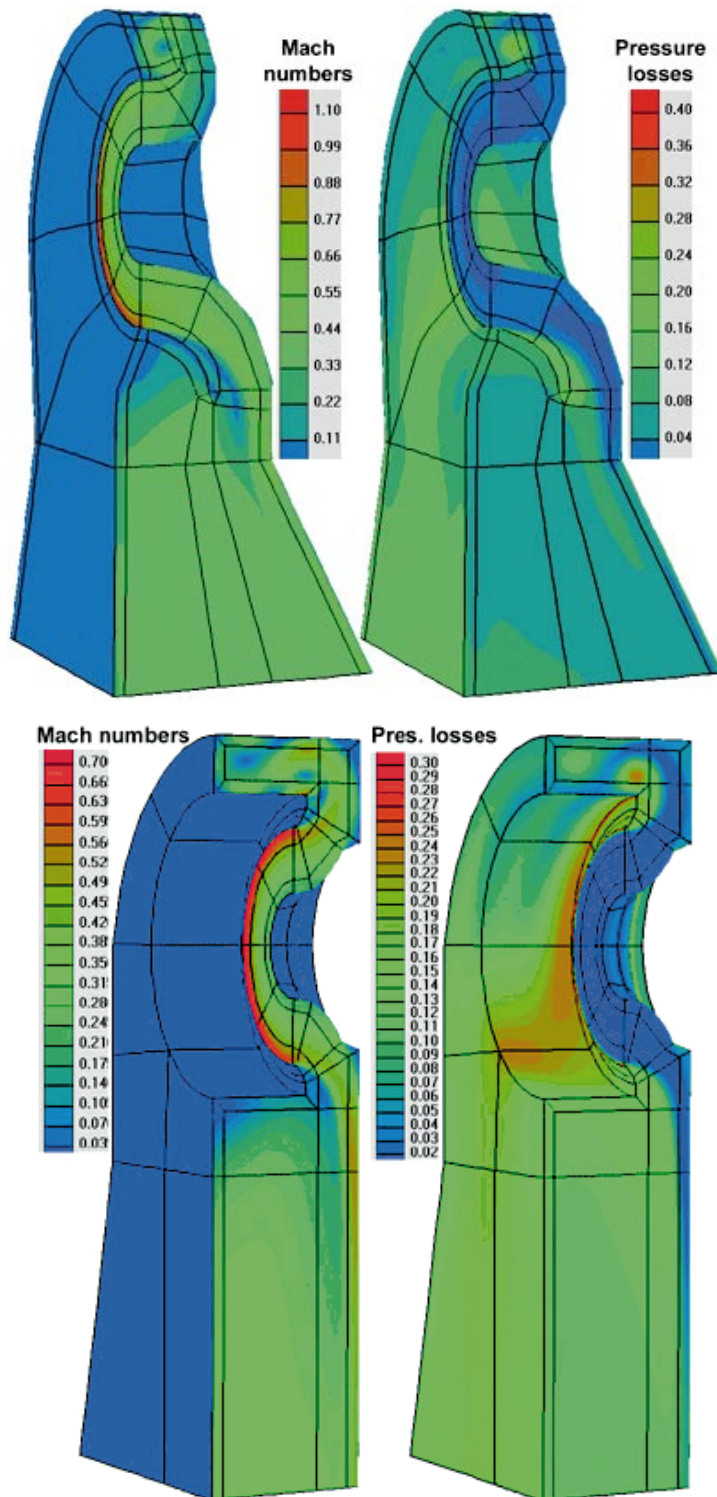**Figure 10.** Tightly fitting mesh for exhaust pipe and outlet chamber of turbounits

V. G. Solodov

Figure 11. Velocity and pressure losses fields for models of K310 (top) and K200 (bottom) turbines exhaust hoods
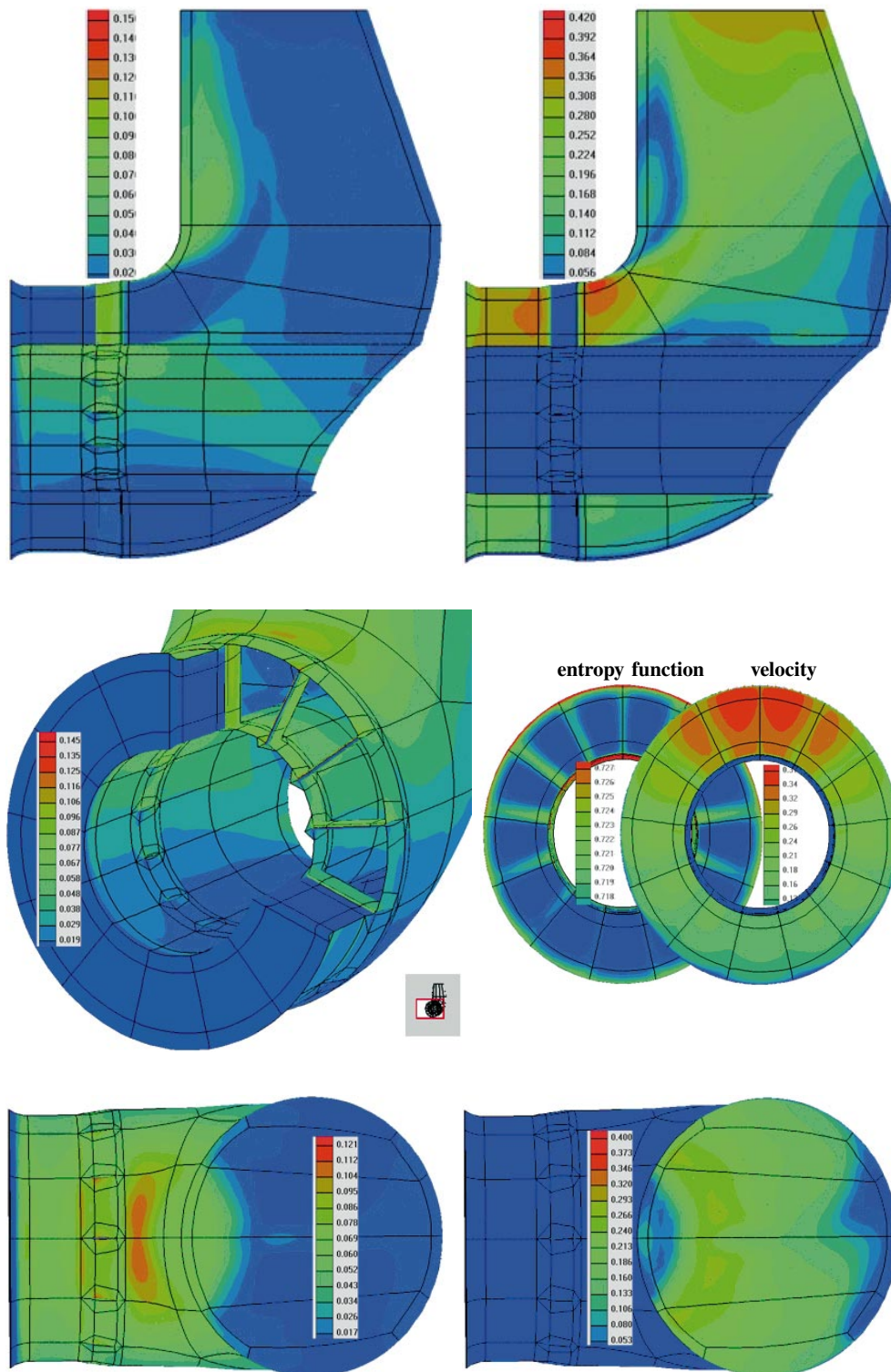
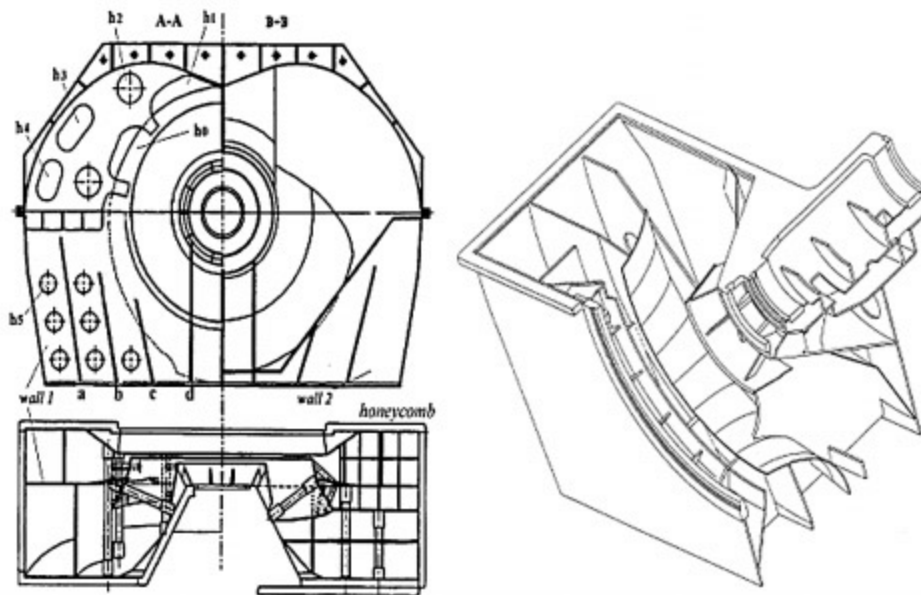**Figure 12.** Pressure losses (left column) and velocity (right column)

Figure 13. Scheme of old design modernized hood

4. Flow model through exhaust comparament "Exhaust Hood-Last Stage"

The experiments [19, 20, 30, 41] show significant periodic nonuniformity of the static pressure (till 20%) in the circular direction behind the last row because of the one-sided exhaust, which leads to reduction of the stage efficiency and appearance of variable low frequency aerodynamic forces on the blading. So the 3D nonstationary flow model of the last turbine stage and exhaust hood interaction is important to study the nonstationary low frequency phenomena occuring in the last stage during the revolution of the rotor.

4.1. Nonstationary 3D model of the last turbine stage-exhaust hood compartment

One of the first simple interaction algorithms was proposed in [30, 31], where the effect of nonuniformity at the inlet plane of the exhaust hood on the nonstationary force characterics at the blading was considered. In [35–37] the full scale aerodynamic coupling procedure was used for the inviscid gas model basing on the fully nonstationary stage model [42]. In [27] the similar coupling procedure was utilized for the viscous gas model with the wall function under the steady stage model. In [28] such a formulation was repeated.

In [26, 35] the phenomenon of shock oscillation was qualitatively simulated along the outer diffuser shell using the ideal gas model and measured data of the tip clearance jet. In works [18, 43] the axisymmetrical model was realized using the viscous gas model, algebraic turbulence model and artificial tip clearance jet model. In [18], viscous nonstationary flow in the diffuser was studied using the Baldwin-Lomax turbulence model, and quantitative agreement with measured data [22] was obtained. The dependence of the unsteady region on the outer diffuser shell, flow regime, tip clearance flow was shown.

According to [27, 31, 35–37] the solution of the problem consists in a coupling calculation procedure based on the full 3D stage model and 3D exhaust hood model
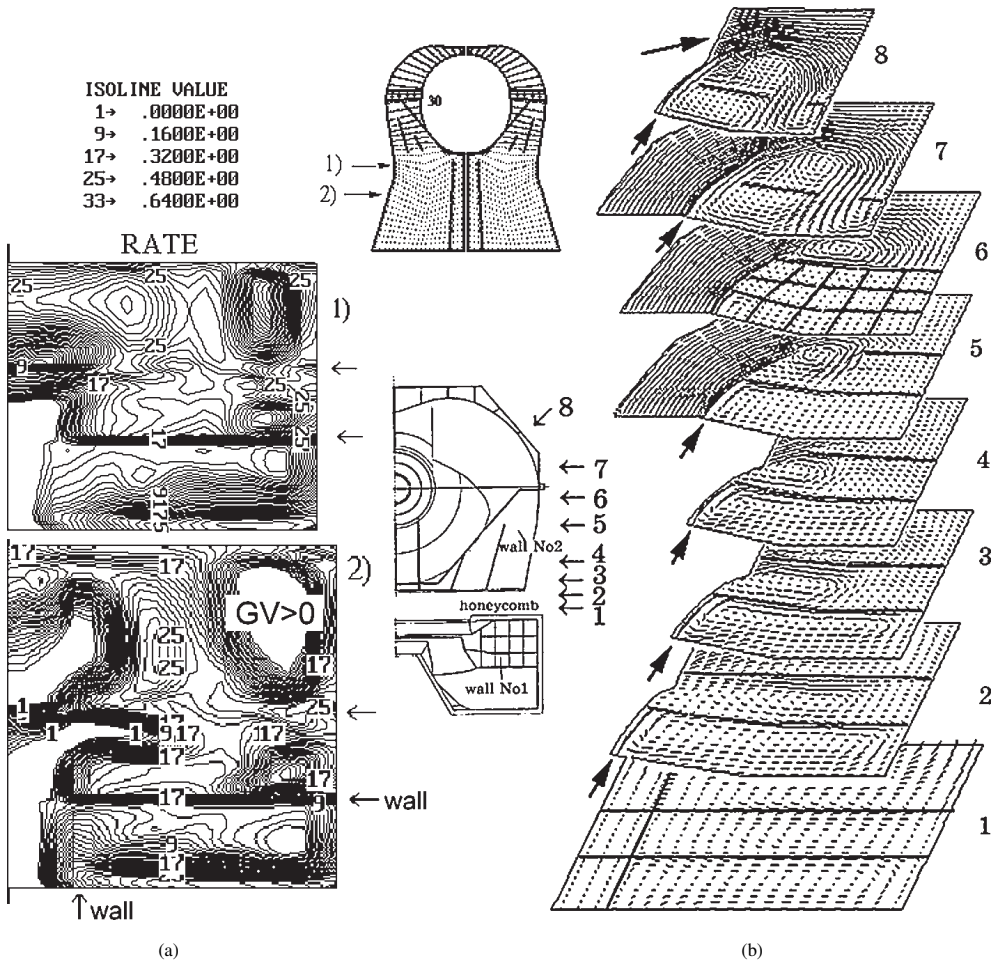
Figure 14. Flow rate (a) and flow pattern (b) in hood of old design after modernization
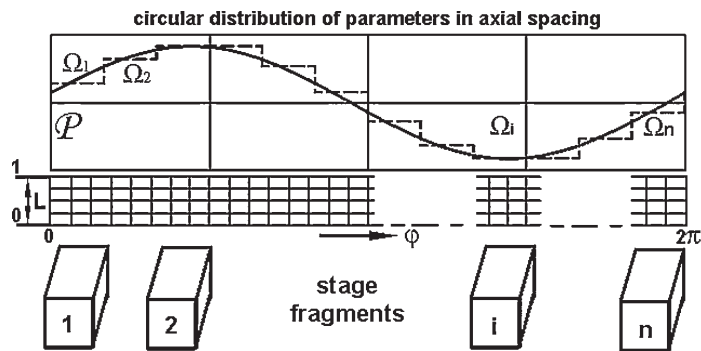

Figure 15. Conception of joining between the stage and exhaust hood

(Figure 15). The calculation region of the stage consists of two interacting channels of the stator and rotor, inlet, outlet interstage spacings. The periodic solution in the calculation region is ensured by integrating the governing equations within the stage periodicity interval.

For the formulation of inlet, exit boundary conditions the usual channel approach is used. For interrow axial spacing the generalized conditions of spacing and periodicity (GSP-conditions) are assigned [42], which take into account the flow pulsation phase shift in the adjacent channels. In the case of the steady stage model, the simple procedure of averaging for the conservative gas-dynamic values of mass, momentum and energy is applied [3].

The most general approach to numerical simulation of exhaust compartment operation supposes the common computational region, being built in the exhaust hood and all channels of stage. But the realization of such approach meets technical difficulties. Namely, as a consequence of difference in scales of volumes of the exhaust hood and stage channel, the spatial division of the exhaust hood has to be sufficiently fine for joining of the exhaust hood and rotor domains. The time needed for getting the periodical flow regime through all channels of the stator and rotor may be equal to the time of several rotor revolutions. The described procedure directly simulates the interaction process of the stage and exhaust hood, but is not acceptable for mass predictions.

The experiments for estimation of circular nonuniformity in the stage-diffuser axial spacing of the exhaust compartment [20, 32, 41] exhibit a sufficiently smooth character of circular distributions of gas-dynamic parameters. This fact leads to the use of quasi-static approach in simulation of stage-exhaust hood interaction, which consists in exclusion of transfer processes in the rotor channels, caused by their movement in the field of large-scale nonuniformity from the exhaust hood. In this case the nonuniformity of fields of gas-dynamic parameters in the stage-diffuser spacing is approximated by a piecewise-constant function (Figure 15), as it was first proposed in [30, 31]. This hypothesis is based on the fact that the ratio of the time interval of particle translation through the rotor channel to the time interval of revolution is essentially less than 1.

Actually, comparing the Strouhal number for the nonstationarity in the interrow spacing due to pitch nonuniformity $St_1 = n z_1 b_2 / w_2$ and its analogue because of large-scale circular nonuniformity from the exhaust hood $St_2 = n b_2 / w_2$, one can see that they differ by z_1 times. Therefore, the flow nonstationarity in the rotor due to nonuniformity behind them is z_1 times less than high frequency nonstationarity due to interaction with the stator blades.

According to the quasi-static approach, every piecewise-constant sector Ω_i is correlated to the corresponding flow in the stage fragment SF_i (Figure 15), being calculated on the basis of constant boundary conditions from Ω_i and under GSP-condition. The general solution for a fixed time point in the stator and rotor domains is given by the superposition of solutions in all stage fragments for all sectors Ω_i.

There are a number of joining models that assure data transfer from the exhaust hood to the stage and in the opposite direction. In papers [27, 37] all conservative gas dynamic parameters are transferred upstream and downstream. The general interaction problem is solved by global iterations in a common time scale with a parameter transfer for every time iteration. The receipt of periodic flow in the stage and steady flow in the exhaust hood is based on the time-marching procedure.

As it has already been mentioned, relatively low circular gradients of parameters in the interstage spacing are a characteristic peculiarity of the stage-exhaust hood interaction. Its exclusion leads to a full stationary model of interaction in the exhaust compartment, which is rigorous for the case of "stage-axisymmetrical diffuser" interaction and is representative to characterize the radial parameter distributions in the interstage spacing. In this case the
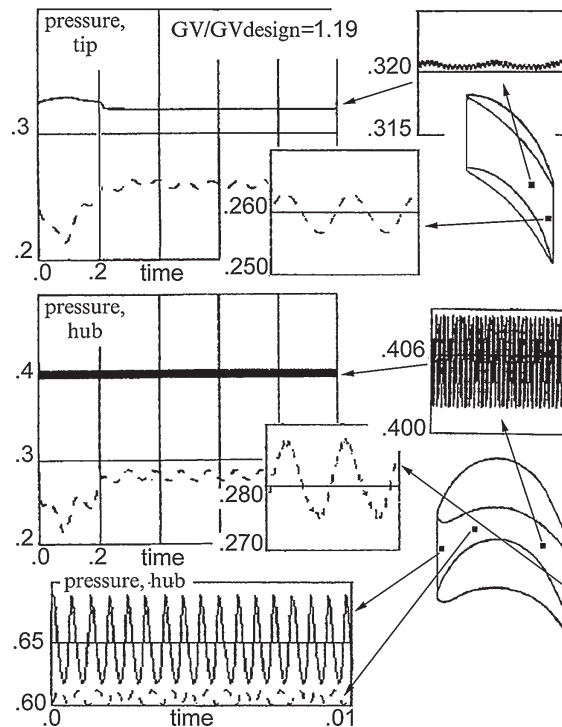
Figure 16. Pressure oscillation in rotor channel (nz_1 and f_p components)

flow is calculated only in a single diffuser sector with parameters from Ω_i under hypothesis of flow axial symmetry. The solution of this problem is found in the 3D computational region of a single stage fragment and corresponding diffuser sector Ω_i.

4.2. Flow nonstationarity in the "stage-exhaust hood" compartment

The general "stage-exhaust hood" model permits us to reveal and separate high frequency (HF) nonstationary phenomena of stator/rotor interaction and low frequency nonstationarity due to non-axial symmetry of the diffuser or exhaust hood. Low frequency (LF) nonstationarity due to possible shocks has a frequency spectrum with an *a priori* unknown range and values of main harmonic frequencies which depend on the inlet swirl, regime, geometry of the outer shell *etc*. These frequencies are not multiple to the rotational frequency, so all the advantages of the quasi-static stage-hood joint model vanish and self-exited oscillations cannot be correctly described in this model.

The phenomenon can be evaluated by the use of the simple stage-axisymmetric diffuser model. This model contains HF nonstationary flow phenomena and LF self-exited nonstationarity for every diffuser section.

Some examples [37] (see also details in [44]) of flow simulation in "stage-diffuser" and "stage-exhaust hood" compartments of the LP cylinder of a "Škoda" old design turbine 500 MW illustrate the nonstationarity of flow parameters in the rotor channel and variable force on the blading.

Figure 16 presents pressure oscillations in points of rotor channel when the compartment operates out of the design regime and the channel is near the horizontal joint. The tip

clearance flow model, being present in the compartment model and based on the experimental data [22], provokes the self-exited flow oscillations in the diffuser, axial spacing and bevel cut domain of the rotor channel of frequency range f_P. In the inlet part of the channel, the HF pressure pulsation due to stator/rotor interaction can be seen. The amplitude of the 1st harmonic of the oscillatory force component on the blade near the horizontal joint is given in Figure 17.
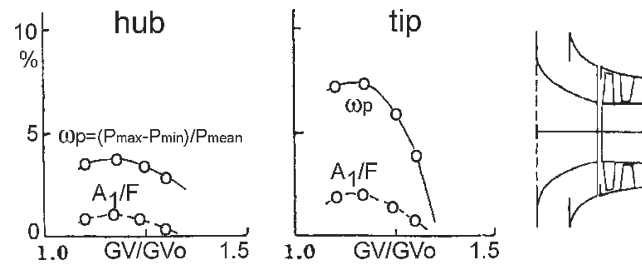
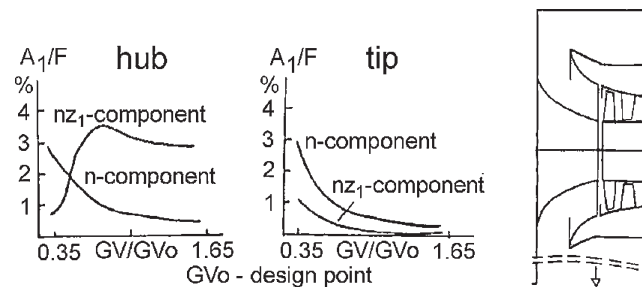**Figure 17.** Amplitude of 1st harmonic of oscillatory force component on blade near horizontal joint

Figure 18. Amplitude of 1st harmonic of HF and LF force component on blading of last compartment

In the case of absence of self-exited flow oscillations, the other two modes of oscillations can be separated. The HF component of the full aerodynamic force over the stage period due to the "stator/rotor" interaction (with nz_1 main frequency) and LF component due to the rotor rotation (with n main frequency) presented in Figure 18, were obtained thanks to the Fourier analysis of full aerodynamic blade force over a full blade revolution. One can see that the absolute values of amplitudes of initial harmonics of the blade force rise when the volumetric rate diminishes, but at the same time the mean blade force A_0 diminishes. For the regular regime the amplitudes of initial harmonics of high frequency pulsation of the full aerodynamic force (FAF) on the stage period are comparable to those of low frequency pulsation of FAF on the rotor revolution. The increase of the volumetric flow rate through the compartment leads to the increase of the velocity at the exit from the stage, and the supersonic zone locked by a shock appears in the outer diffuser shell. For such high load regimes, the flow in the bevel cut becomes supersonic and the disturbances up to flow are getting weaker. These regimes are accompanied by the rise of vorticity near the horizontal joint and M_{C2}, but at the same time the diminishing of the circular nonuniformity in the axial spacing occurs.

5. Conclusion

Some recent advances in computational gas dynamics of exhaust diffusers are presented. The compressor/turbine axial-radial exhaust diffusers and outlet devices of compressor/turbine units, exhaust hoods for power steam turbines are considered. The formulations of problems for CFD analysis of these devices are discussed including the coupling procedure for joint operation of the last stage and exhaust hood. The numerical implementation of differential turbulence model is described. The new approach is developed to the description of computational domain and parallel numerical solution of transport equations based on the unstructured set of structured grid blocks with tightly fitting meshes.

References

[1] Lapin Y V and Strelets M H 1989 *Internal Flows of Gas Mixtures* Moscow, Nauka p. 366 (in Russian)

[2] Solodov V G and Starodubtsev Y V 2001 *The Mathematical Modelling of Viscous Compressible Turbulent Flow in Channels of Complex Shape* Vestnik of Kharkov National University **129** p. 9 (in Russian)

[3] Rusanov A and Yershov S 1996 *The new implicit ENO method for 3D viscous multi stage flow calculations* Proc. 3rd ECCOMAS Computational Fluid Dynamics Conf., September 9–13 1996, Paris, France, pp. 911–916

[4] Yershov S V 1994 *Math. Model.* **6** (11) 63 (in Russian)

[5] Fletcher C A J 1988 *Computational Techniques for Fluid Dynamics. Fundamental and general techniques* Springer-Verlag, Berlin, p. 504

[6] Yershov S V 1998 *Problems in Mechanical Engineering* (Problemi Machinostroenia) **1** (2) 76 (in Russian)

[7] Bardina J E, Huang P G and Coakley T J 1997 *Turbulence Modeling Validation, Testing, and Development* NASA TM 103931, p. 98

[8] Spalart P R and Allmaras S R 1992 *A One-Equation Turbulence Model for Aerodynamic Flows* AIAA Paper 92–0439, p. 21

[9] Zaitsev D K, Nikolaev V V, Riess V V and Smirnov E M 2000 *Numerical Simulation of Turbulent Separated Flows in Axial Radial Turbine Diffusers* In book: Upgrading of Turbines by the Mathematical and Physical Methods, Kharkov, Institute for Problems in Machinery, NAS of Ukraine, pp. 257–264 (in Russian)

[10] Solodov V G and Starodubtsev Y V 2000 *The Solver for Numerical Solution of 3D Unsteady Internal Gas Dynamic Problems* KhSAHTU Technical and Scientific Reports (11–12) pp. 101–103 (in Russian)

[11] Rusanov A V, Yershov S V and Kudrinskiy A V 1998 *The Uniform Algorithm of Flow Simulation in Complex Domains of Arbitrary Shape* Proc. of 3rd Congress of Ukrainian Engine Designers, Kiev, pp. 100–103 (in Russian)

[12] Rusanov V V, Solodov V G, Starodubtsev Y V and Yershov S V 2001 *The uniform numerical technique for multiblock CFD solver* Proc. of 5th Int. Symp. Exper. and Comput. Aerothermodynamics of Internal Flows (to be published)

[13] Monson D J and Seegmiller H L 1992 *An Experimental Investigation of Subsonic Flow in a Two-Dimensional U-Duct* NASA TM 103931

[14] Bachalo W D and Johnson D A 1979 *An Investigation of Transonic Turbulent Boundary Layer Separation Generated on an Axisymmetric Flow Model* AIAA 79–1479

[15] Dominy R G, Kirkham D A and Smith A D 1998 *Transactions of the ASME* **120** 298

[16] Hirsch C 1990 *Numerical Computation of Internal and External Flows* **1, 2**, N.Y., Jonh Wiley&Sons

[17] Fric T F, Villarreal R, Auer R O, James M L, Ozgur D and Staley T K 1998 *Transactions of the ASME* **120** 186

[18] Merz R, Mayer J, Stetter H and Kruekels J 1995 *Computation of Three-Dimensional Viscous Transonic Turbine Stage Flow Including Tip Clearance effects* ASME Paper 95-GT-76

[19] Migaj V K and Gudkov E I 1981 *Calculation and Design of Exhaust Diffusers of Turbomachines* Leningrad, Machinostroenie p. 271 (in Russian)

[20] Simoyu L L, Lagun V P and Boytsova E A 1991 *Teploenergetika* **2** 28 (in Russian)

[21] Zariankin A E, Simonov B P, Paramonov A N and Chusov S A 1998 *Teploenergetika* **1** 20 (in Russian)

[22] Maier R 1989 *Experimentelle Untersuchung Selbsterregter Stoss-Grenzschicht-Pulsationen in Abdampfdiffusoren* Dissertation, Universitat Stuttgart, p. 167

[23] Maier R and Wachter J 1988 *ASME Journal of Turbomachinery* **110** 173

[24] Gnesin V I and Solodov V G 1994 *Numerical Simulation of Oscillatory Instabilities in Turbines Axial-Radial Diffuser Flow* Proc. of the 7th ISUAAT, Kyushy, Japan (Ed.:Y.Tanida,M.Namba), pp. 661–674, Elsevier Sci. BV.1995

[25] Solodov V G 1996 *Nonstationary 3D Inviscid Numerical Flow Model Through Steam Turbine Exhaust Hood* Proc. 3rd Int. Colloquium on Process Simulation, Espoo, Finland, pp. 89–110

[26] Solodov V G and Gnesin V I 1997 *Journ. of Thermal Sciences* **6** (4) 231

[27] Benim A C, Geiger M, Doehler S, Schoenenberger H and Roemer H 1995 *Modelling the Flow in the Exhaust Hood of Steam Turbines Under Consideration of Turbine-Exhaust Hood Interaction* VDI Berichte (1185) pp. 343–357

[28] Dejean F, Bourdouneau L, Denis C and Duplex J 1997 *Three-Dimensional Coupled Flow Calculations in a Low Pressure Steam Turbine Last Stage and Exhaust Hood* 2nd European Conf. on Turbomachinery, Fluid Dynamics and Thermodynamics Antwerpen, Belgium, 5–8 March 1997, Belgium, pp. 347–354

[29] Gardzilewicz A and Solodov V G 1999 *Spatial Unsteady Flow Pattern in an Old-Design 200MW Turbine Exhaust Hood and Ways of Its Improvement* Turbomachinery (Cieplne Maszyny Przepływowe), Politechnika Łódzka **115** 139

[30] Gnesin V I and Solodov V G 1988 *Teploenergetika* **4** 22 (in Russian)

[31] Gnesin V I and Solodov V G 1993 *Turbine Stage Aerodynamical Interaction with Supplying and Rejecting Devices of Flow Path* Proc. of Int. Symp. on Exp. and Comput. Aerothermodynamics of Internal Flows, Prague, Czech Rep., pp. 243–248

[32] Łuniewicz B, Gardzilewicz A, Zariankin A, Marcinkowski S, Solodov V, Sowa R and Karbowski M 1997 *Modernization of the 200MW Turbine Exhaust Hood* Proc. of IMP'97, Modelling and Design in Fluid-Flow Machinery Conf., J. Badur *et al.* eds., IMP PAN Publishing, Gdansk, Poland, pp. 33–45

[33] McCloskey T H, Dewey R P and Hesler S H 1995 *Low Pressure Steam Turbine Thermal Performance Improvements* EPRI 4th Nuclear Plant Performance Seminar, p. 11

[34] Solodov V G 1994 *The Problems in Mechanical Engineering* (Problemi Machinostroenia) **40** 41 (in Russian)

[35] Solodov V G 1995 *The Foundations of Mathematical Modelling of Aerodynamical Interaction of Turbine Stage Aerodynamical Interaction with Supplying and Rejecting Flow Path Devices* Dissertation (Habilitation), Kharkov, Politechnical University, p. 310

[36] Solodov V G 1995 *Numerical Simulation of Unstable and Oscillatory Flow Regimes in Steam Turbine Exhaust Systems* Proc. 3rd ICIAM (Regensburg, Germany, 1995) ICIAM95 446 Hamburg, Germany

[37] Solodov V G and Gnesin V I 1995 *Nonstationary 3D Numerical Model of Last Turbine Stage-Exhaust Hood Aerodynamical Interaction* Proc. 1st European Conf. „Turbomachinery — Fluid Dynamic and Termodynamic Aspects", Erlangen, Germany, p. 14; also VDI Berichte (1185) 359–373

[38] Solodov V G 1998 *Numerical Approach to Study the Non-Stationary Flow Phenomena in „Exhaust Hood-Last Stage" Compartment* Transactions of the Institute of Fluid-Flow Machinery **105** 33

[39] NPP Mashproekt, Technical Report 2001 Nikolaev, p. 20 (in Russian)

[40] Solodov V G, Starodubtsev Y V, Bucholdin Y S and Levashov V A 2000 *The Aerodynamical Improvement of Inlet and Outlet Devices of Axial-Radial Compressor with use 3D CFD Analysis* In book: Upgrading of Turbines by the Mathematical and Physical Methods, Kharkov, Institute for Problems in Machinery, NAS of Ukraine, pp. 257–264 (in Russian)

[41] Garkusha A V 1983 *Aerodynamics of Flow Path of Steam Turbines* Moscow, Machinostroenie p. 184 (in Russian)

[42] Gnesin V I 1982 *Izvestia AN SSSR. Mechanika Zhidkosty i Gaza* **6** 138 (in Russian)

[43] Lampart P, Gardzilewicz A, Yershov S and Rusanov A 2000 *Investigations of flow characteristics of an HP turbine stage including the effect of tip leakage and windage flows using a 3D Navier-Stokes solver with source/sink-type boundary conditions* Proc. 2000 Int. Joint Power Generation Conf., Miami Beach, Florida, July 23–26, IJPGC2000-15004

[44] Stastny M 1989 *Maschinenbautechnik* **38** (1) 27